Deconstructing the Local Intermolecular Ordering and

Dynamics of Liquid Chloroform and Bromoform

 $John. \ J \ Karnes^{a,*} \ and \ Ilan \ Benjamin^{b,*}$

^aLawrence Livermore National Laboratory, Livermore, CA 94550, United States; ^bDepartment of Chemistry and Biochemistry, University of California-Santa Cruz, Santa Cruz, CA 95064, United States

KEYWORDS. haloforms, molecular dynamics, spatial distribution function, polar liquids, liquid structure, molecular liquids, polar stacking

ABSTRACT. Local intermolecular structure and dynamics of the polar molecular liquids chloroform and bromoform are studied by molecular dynamics simulation. Structural distribution functions, including 1- and 2-D pair correlations and dipole contour plots allow direct comparison and show agreement with recent analyses of diffraction experiments. Studies of the haloforms' reorientational dynamics and longevity of structural features resulting from intermolecular interaction extends previous work toward deeper understanding of the factors controlling these features. Analyses of ensemble average structures and dynamical properties isolate mass, electrostatics, and steric packing as driving forces or contributing factors for the observed ordering and dynamics.

1. Introduction

Hard-sphere, atomic, and molecular liquids composed of small molecules with high symmetry are particularly attractive systems of study since their intra- and intermolecular geometries and ordering suggest a limited set of degrees of freedom and the potential for straightforward conceptualization and visualization.¹⁻⁶ Deepening and clarifying the understanding of well-known, high-symmetry neat molecular liquids serves as a building block toward insights into the structure of more complex molecular species and multi-component liquid systems. Additionally, both the insights and analysis techniques validated by the investigation of neat liquids are readily extendable to the study a molecular liquid's organization around a solute and at interfaces between the molecular liquid and an adjacent, dissimilar phase. Diffraction experiments, computer simulations, and data analysis techniques applied to the study of neat molecular liquids continue to evolve and reveal new, increasingly detailed insights that both confirm and challenge earlier work.⁷⁻¹⁵

Early insight into the ordering and structure of molecular liquids by van der Waals forces was summarized by Chandler, 16,17 "the harsh repulsive forces (which are nearly hard core interactions) dominate the liquid structure. Stated in other words, the shape of molecules determines the intermolecular correlations." This central theme, that steric effects and local packing are far more important than attractive forces and dipole-dipole interactions, was then pursued quantitively in development of the Weeks-Chandler-Anderson (WCA) potential which, to some approximation, treats the attractive component of the Lennard-Jones potential as a small perturbation. This description of molecular liquids' structure has obvious limitations when the attractive forces are large and quickly vary (as a function of particle separation) as in the case of hydrogen bonding in water or coulombic interactions of molten salts. A less obvious

limitation is the occasional propensity for attractive forces to produce structural effects that do not compete with the strong repulsive forces, which may be the case in molecular liquids that possess nontrivial dipoles.

The haloform molecules, most notably chloroform (CHCl₃) and bromoform (CHBr₃) exemplify the above description. Both molecules belong to the C_{3y} symmetry group, with nearlytetrahedral geometries and possess well-defined molecular dipole vectors that are readily approximated by the C-H vector. Theoretical and computational approaches toward describing the local structure and orientation of haloforms have often focused on the importance of forces outside the 'harsh repulsive' class since these molecules serve as a clear, accessible example of molecular liquids whose characteristic intermolecular ordering and dynamics should inhabit the space between hard sphere and hydrogen bonded liquids like water. Early computational work represented haloform molecules as a single-site Lennard-Jones liquid and produced radial distribution functions (RDF) that agreed with scattering data reasonably well.²¹ With increasing computational resources, all-atom molecular dynamics simulations came within reach and the accuracy of predicted local molecular structure increased by accounting for the molecules' deviations from spherical symmetry. Polarizable models provided further accuracy at the cost of additional computational expense and allowed for more precise simulation of chloroform's behavior in solvent/solute and interfacial systems.^{22–24} We refer the reader to a recent review by Pusztai and co-workers for a more complete discussion of computational and theoretical approaches.²⁵ The local intermolecular ordering of these haloforms has been investigated in several studies over the last few decades^{25–29} and has recently received additional attention with the detailed neutron diffraction-empirical potential structure refinement (ND-EPSR) studies performed by Salzmann and co-workers. 30,31

Salzmann and co-workers hypothesize that the local intermolecular order of haloform molecules may influence and impart some of the interesting and sought-after solvation properties. Their neutron diffraction study of chloroform presents a detailed but concise summary of intermolecular ordering and dipole-dipole orientational correlation by implementation of spatial distribution functions (SDF) and orientational contour plots. Most of the analysis agrees with and confirms earlier studies with one major difference: At low intermolecular distances parallel dipole alignments are by far the most dominant structure.³⁰ This is in contrast to earlier diffraction studies reporting that the dominant short-range structural feature is antiparallel, where fully chlorinated faces of two tetrahedral molecules approach each other.^{29,32} Additionally, Salzmann and co-workers introduce the definition of a 'polar stack,' reminiscent of the 'Apollo configuration,' where neighboring CHCl₃ molecules have parallel and colinear dipoles with one molecule's hydrogen atom positioned in the hollow formed by the neighbor molecule's three chlorine atoms.^{27,30} Our molecular dynamics simulations of liquid chloroform agreed with the reported population and population distribution of these polar stacks but also suggested that these structures are a result of steric packing, not electrostatic interactions.³³ Salzmann and co-workers recently followed their CHCl₃ work with a similarly detailed ND-EPSR analysis of liquid CHBr₃, that builds upon earlier scattering-reverse Monte Carlo studies^{28,29} by elucidating detailed angle-dependent pair correlations (SDFs) and dipoledipole orientational correlations.³¹ These two experimental studies suggest structural similarity but a greater tendency for antiparallel alignment in CHBr₃ than in CHCl₃, a phenomena the authors attribute to stronger halogen bonding or weak but persistent long-range orientational correlations. These recent findings revisit the second, less obvious type of exception from the

van der Waals picture of molecular liquids: That weaker interactions may produce structural effects that do not compete with the short-range strong repulsive/steric interactions.¹⁷

In light of these recent findings, we extended our molecular dynamics simulations of chloroform to study liquid bromoform with new data analysis techniques that will allow us to directly compare our simulation results to these recent diffraction experiments and add dynamic insight. Additionally, we use a well-known force field to model the haloforms whose piecewise form allows us to systematically disable contributions to the interaction potential to isolate contributions to the local structure and ordering in the liquid haloforms.

2. Simulation details

Neat bromoform and chloroform liquids are simulated by 794 molecules in truncated octahedron boxes, whose enclosing cubes have an edge length of 61.32 Å for bromoform and 59.69 Å for chloroform, reproducing the experimentally known densities of these liquids at 298K. The truncated octahedron box, shown in Figure 1a, tessellates 3-dimensional space and its boundaries more closely approximate the radial geometries of most interaction potentials than a cubic box. Selection of the truncated octahedron geometry therefore results in simulations with the same characteristic size as simulations performed in the corresponding enclosing cubic box with a factor of 2 fewer particles, resulting in a significant reduction in computational expense and precisely the same results and statistics for spherically symmetrical calculations. Figure 1b is a representative simulation snapshot of the CHBr₃ system. Each molecule is represented by 5-site, fully flexible, fixed-charge models where the intermolecular interaction potential is the pairwise sum of Lennard-Jones and Coulombic terms

$$u_{ij} = 4\varepsilon_{ij} \left[\left(\frac{\sigma_{ij}}{r} \right)^{12} - \left(\frac{\sigma_{ij}}{r} \right)^{6} \right] + \frac{q_i q_j}{4\pi r \varepsilon_0} \tag{1}$$

where r is the distance between atom centers i and j. We use the OPLS-AA force field ³⁴ with partial charges generated by the 1.14*CM1A-LBCC approach ^{35–37} to represent each haloform molecule. A full listing of the inter- and intramolecular potential energy parameters is shown in Tables 1 and 2. This force field differs from our previous study of chloroform ³³ and this change was mostly motivated by the need for consistent parameterization between the two haloform species. Classical molecular dynamics simulations and subsequent analyses were performed using in-house code, which implements the velocity Verlet algorithm. Ten independent starting configurations were generated by randomly placing haloform molecules into the simulation boxes and relaxing each simulation box for over 1 ns before initiating production runs. Spatial distribution functions, dipole orientation contour plots, and all other data presented in this work were calculated on-the-fly and represent an ensemble average of 10^6 configurations collected during 10 ns of simulation time.

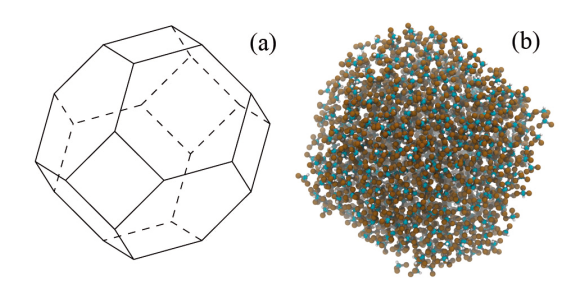


Figure 1. (a) Wireframe depiction of truncated octahedral periodic boundaries and (b) corresponding molecular dynamics simulation snapshot of liquid bromoform that implements this geometric boundary.

Table 1. Intermolecular Potential Parameters Used in the CHX₃ Models

Atom	σ(Å)	ε (kcal/mol)	<i>q</i> (e)
C_{BFM}	3.50	0.066	0.1063
Br	3.47	0.047	-0.099
H_{BFM}	2.50	0.030	0.1907
C_{CFM}	3.50	0.066	0.3792
Cl	3.40	0.300	-0.1873
H_{CFM}	2.50	0.030	0.1827

 Table 2. Stretch and Bend Equilibrium Values and Force Constants

Equilib. value	Force const. (× kcal/mol)
$r_{CBr}^{eq} = 1.945 \text{ Å}$	$k_{CBr} = 490.0 \text{ Å}^{-2}$
$r_{CH}^{eq} = 1.090 \text{ Å}$	$k_{CH} = 680.0 \text{ Å}^{-2}$
$\theta_{BrCBr}^{eq} = 111.7^{\circ}$	$k_{BrCBr} = 156.0 \text{ rad}^{-2}$
$\theta_{BrCH}^{eq} = 107.6^{\circ}$	$k_{BrCH} = 102.0 \text{ rad}^{-2}$
$r_{CCl}^{eq} = 1.781 \text{ Å}$	$k_{CCl} = 490.0 \text{ Å}^{-2}$
$r_{CH}^{eq} = 1.090 \text{ Å}$	$k_{CH} = 680.0 \text{ Å}^{-2}$
$\square_{CICCI}^{eq} = 111.7^{\circ}$	$k_{ClCCl} = 156.0 \text{ rad}^{-2}$
$\theta_{CICH}^{eq}=107.6^{\circ}$	$k_{CICH} = 102.0 \text{ rad}^{-2}$

3. Results and discussion

3.1 Overview of local structure: Spatial distribution functions

Figure 2 shows selected radial distribution functions (RDFs) for the neat chloroform and bromoform liquids. Bromoform is represented by orange curves and chloroform by green curves.

RDFs are calculated as

$$g_{\text{A-B}}(r) = \frac{1}{\eta_c} \langle \sum_{i=1}^N \delta(r - r_i) \rangle \tag{2}$$

where r_i is the distance between atom centers A and B, δ is the Kronecker delta, η_c is a normalization factor proportional to the number of particles in a spherical shell with radius r at bulk density ρ , 38 and the ensemble average is collected over all N molecules and all possible reference atoms. In practice the RDF is calculated as nested spherical shells centered at equally spaced r with finite width dr. This width defines the resolution of the RDF. Since the two haloforms share C_{3v} symmetry, steric character (one hydrogen and three halogens), and an overall nearly-tetrahedral geometry, similarity between their corresponding RDFs is expected. These RDFs agree well with neutron diffraction data and previous simulations that employ a polarizable model force field.^{22,30,31} Figure 2a shows the RDFs of the central carbon atoms, in which each haloform shows local ordering extending to three solvation shells, with peaks at approximately 5, 10, and 15 Å. Due to bromoform's larger size the bromoform curve is shifted slightly toward larger values than chloroform with the first peaks at 5.3 and 5.5 Å. Aside from this shift and a slight broadening of the bromoform peaks, the two $g_{C-C}(r)$ curves are very similar. Figures 2b and 2c show the carbon-hydrogen and carbon-halogen RDFs for the haloforms. The first C-H solvation shell appears as a doublet in both liquids, with bromoform's first peak slightly smaller than the corresponding feature in the chloroform $g_{C-H}(r)$. Similar to 2a, the bromoform curve is shifted toward larger r by about 0.3 Å. The peaks indicating a more complex local ordering of C-H than the C-C curves in Figure 2a. Similarly Figure 2c shows a more complex structure, a broad first solvation peak followed by a smaller shoulder. While not definitive, the curves in Figure 2 suggest that important features of the local ordering may not be captured by conventional RDFs, whose description is limited to being radially symmetrical.

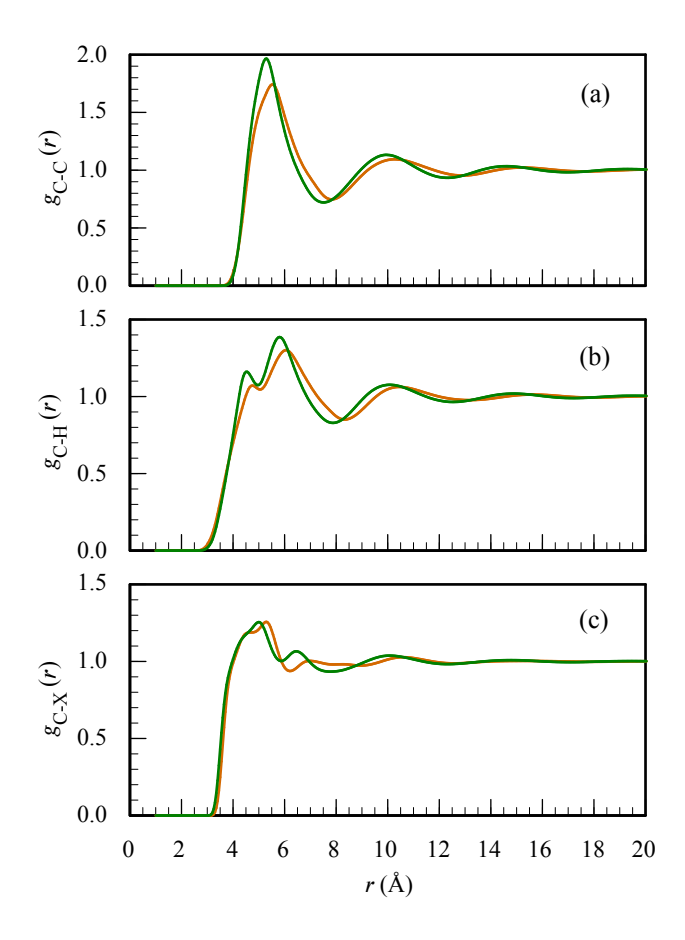


Figure 2. Radial distribution functions for neat liquid bromoform (orange) and chloroform (green).

To remove this limitation, we add an angular component to Equation 2 and define a spatial distribution function (SDF) as

$$g_{\text{A-B}}(r,\theta) = \frac{1}{\eta_a} \langle \sum_{i=1}^N \delta(r - r_i) \cdot \delta(\theta - \theta_i) \rangle$$
 (3)

where θ is the angle formed by two vectors that originate at the reference molecule's central carbon atom and point toward the reference molecule's hydrogen and the atom center of interest in the neighboring molecule. The normalization factor η_a is the number of particles in the ring defined by r and θ at bulk density ρ . Analogous to the RDF, each pixel in the SDF represents a section of the spherical shell of width dr, centered at radius r, spanning an angular range $d\theta$ and

centered about θ . Figure 3a shows a schematic that defines the variables r and θ and Figure 3b illustrates the relationship between the SDFs and RDFs as defined in this work, where the RDF is a projection of the SDF from the r- and θ -axes onto the r-axis. In the case of g_{C-C} , the SDF reveals that the first density peak represents an inhomogeneous, non-spherical region of high density that collapses into a single peak when projected onto one dimension. This first peak in the RDF is mostly populated by a high-density region centered at approximately $\theta = 180^{\circ}$ and the tail of this peak is a separate region at $\theta = 30^{\circ}$.

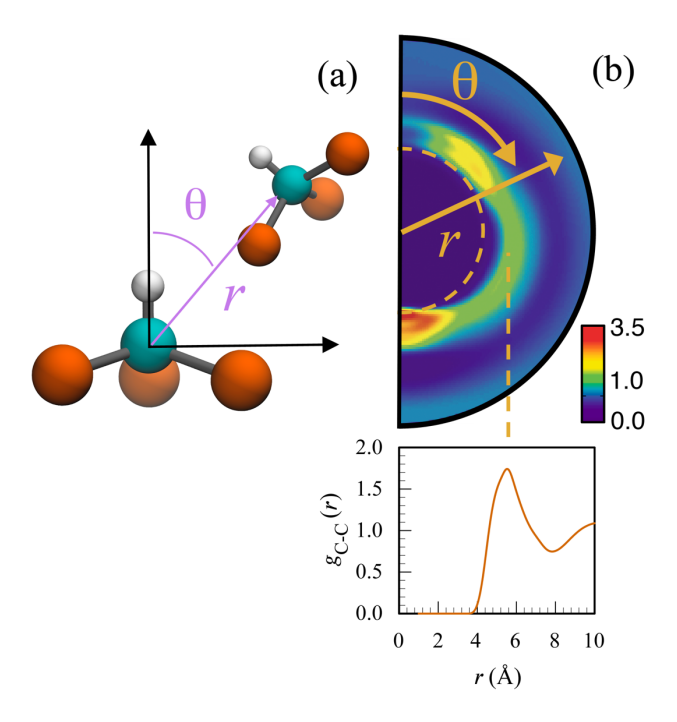


Figure 3. (a) Cartoon schematic illustrating the variables r and θ pertaining to $g_{\text{C-C}}(r,\theta)$. (b) The spatial distribution function $g_{\text{C-C}}(r,\theta)$ is presented with its one-dimensional projection onto $g_{\text{C-C}}(r)$. The radius of the $g_{\text{C-C}}(r,\theta)$ contour corresponds to the x-axis of the RDF.

Figure 4 shows chloroform and bromoform SDFs side-by-side to facilitate direct comparison.

A ball-and-stick model of a representative haloform molecule is overlaid in the approximate position of the reference molecule in these calculations, which extend to a maximum radius of 10

Å. The two central bands of high $g(r, \theta)$ value in the SDFs correspond to the first solvation shells of the RDFs in Figures 2b and 2c, where the more central band represents the case where the neighboring atom center of interest is positioned closest to the reference atom. The outer or second sub-shell band accounts for molecules where the SDF atom center is positioned away from the reference atom. The overall similarity of the haloform SDFs, despite chlorine atoms being 0.088 e more negative than bromoform's bromine atoms, is an indication that local ordering is a strong function of packing effects. Both pairs of SDFs show very good overall agreement with the recent ND-EPSR results of Salzmann and co-workers^{30,31} and our analysis of the SDFs in Figure 4 will detail the differences observed.

Figure 4a shows carbon-hydrogen SDFs for the chloroform and bromoform liquids and corresponds to the RDFs in Figure 2b. Although the RDFs appear quite similar, aside from a slight shift due to bromoform's larger size, the SDFs reveal more differences between the halogens' local intermolecular ordering. The most notable of these differences is the position of nearest neighbor hydrogens around the halogen sites, $90^{\circ} < \theta < 180^{\circ}$. In chloroform, this first band of $g_{\text{C-H}}(r,\theta)$ is at a maximum between 100° and 165° . Bromoform shows a similar band but its density is more localized and centered around $\theta = 180^{\circ}$, indicating the greater likelihood of a neighboring hydrogen atom to be located in the hollow formed by the three bromine atoms. This difference in local ordering is particularly noteworthy because the chlorine atom centers carry more negative partial charges than the bromine atom centers. Although steric packing is the primary driver of intermolecular ordering in the haloforms, the low density region around the reference hydrogen is a result of electrostatic repulsion, confirmed in our earlier simulation work³³ and presented in greater detail by Figures S1 and S2 in the Supporting information, which juxtapose these SDFs with analogous haloform simulations performed with all partial charges set

to zero. The ordering of the second $g_{\text{C-H}}(r, \theta)$ subshells is much more similar, with high density regions centered at approximately 30° and 180°, these bands combining to form the larger second peak of the first solvation shell doublets in Figure 2b.

Figure 4b shows carbon-halogen SDFs for the chloroform and bromoform liquids. To a first approximation the two SDFs look identical and share high-density regions in the first and second solvation shells that correspond to the hollows formed by the triangular faces of the tetrahedral haloforms centered at approximately 25° (H-X-X) and 180° (X-X-X). The longer C-X bonds and larger halogen van der Walls radius in bromoform shift the first and second solvation shells further from the central atom and result in more distortion of the band representing the first solvation shell away from circular shape. These differences appear subtle in the juxtaposed SDFs but are more clear in the RDFs in Figure 2c, particularly the broadened and shifted second peak of bromoform.

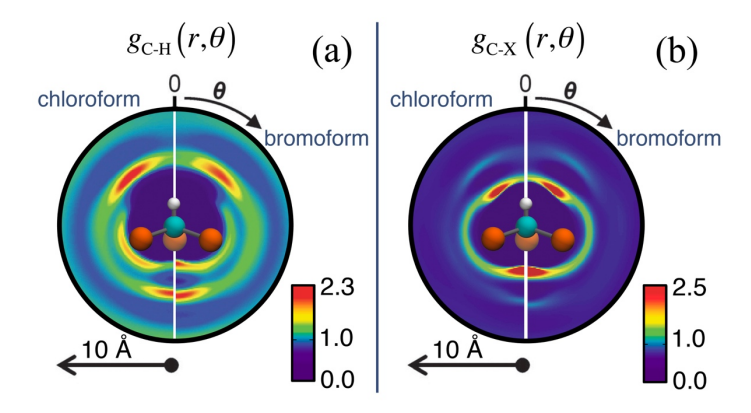


Figure 4. Comparison of chloroform and bromoform spatial distribution functions obtained by molecular dynamics simulations. Images consider (a) carbon-hydrogen $(g_{C-X}(r,\theta))$ and (b) carbon-halogen $(g_{C-X}(r,\theta))$ ordering of the two haloforms.

As complementary analysis and to enable more direct comparison of these simulations with recent ND-EPSR work,^{30,31} we consider the relative orientation of the halogens' dipole vectors as

a function of their position. Figure 5 shows dipole orientation contour plots for the two haloform liquids. Each semicircular or circular contour in Figure 5a-b summarizes the orientation of the local neighbors' dipole vector when located at a specified angle θ relative to the central reference molecule i. Values of 0° , 45° , 90° , 135° , and 180° were selected to survey θ for bromoform and chloroform. Figure 5c is a cartoon schematic that defines r_{ij} as the distance between haloforms i and j, the angle θ , and the angle α formed by the diploe vectors $\vec{\mu}_i$ and $\vec{\mu}_j$. Figure 5d shows 4 intermolecular configurations that correspond to the positions in the contour plots in Figure 5a labeled (1)-(4) to assist in the interpretation of these contour plots.

The dipole orientation contour plots in Figure 5 are in good general agreement with those recently reported by Salzmann and co-workers. 30,31 The contour plots are similar for both haloforms, with one or more preferred orientations for each value of θ that may be explained in steric or electrostatic terms. In all orientations and in both liquids these MD simulations show an orientational preference for the neighboring dipole moment vector to be parallel to the vector \vec{r}_{ij} , also in agreement with the recent series of ND-EPSR studies. These MD simulations also show preference for $\alpha \approx 235^{\circ}$ in the $\theta = 90^{\circ}$ contours and at $\alpha \approx 300^{\circ}$ and $\alpha \approx 350^{\circ}$ for $\theta = 135^{\circ}$. These preferred orientations are enhanced by electrostatic interaction, the attraction of the neighboring hydrogen to the halogen atoms and repulsion of the halogens by the reference molecule's halogens. Analogous to our deconstruction of the SDFs, we confirm that electrostatics induce this ordering by again comparing with simulations where the partial charge of each atom center in the simulation is set to zero. Figure S3 in the Supporting Information shows a set of dipole orientation contour plots calculated for both haloform liquids with the electrostatic contribution to the potential removed. These 'q = 0' simulations also reveal that electrostatic interactions are important in the $\theta = 45^{\circ}$ case, where orientational preference is shown at $\alpha \approx 255^{\circ}$ in the zero

charge simulations but not in the corresponding contours shown in Figure 5a-b. Previous related simulation work has emphasized sterics over electrostatics as the dominant factor in the overall local ordering of these haloforms; 33,39 this example shows cases where electrostatics impact local intermolecular orientation. We reemphasize that this work uses a fixed-charge force field that may overemphasize the locality of electrostatic effects and include the q=0 simulations so these two sets of MD simulations may serve as endpoints representing fixed and diffuse electrostatics in these polar liquids and refer the reader to Section S1 of the Supporting Information for further discussion.

The cases of $\theta = 0^{\circ}$ and $\theta = 180^{\circ}$ are of particular interest since they provide a deeper investigation into the "chain-like" arrangements²⁹ of these two molecular liquids. This chain-like arrangement has been of interest for decades, beginning with suggestions of an 'Apollo configuration' in liquid chloroform, described as nearest-neighbor chloroform molecules having parallel, collinear dipoles with the hydrogen atom being located in the "hollow formed by three chlorine atoms."27 The Apollo configuration was dismissed as a minor contribution to haloform structure, 25,40 but recent experiments and simulations have continued investigating this arrangement by considering chains of head-to-tail dipoles, "polar stacks," where the H-C···H angle is 180±30°, as opposed to parallel, collinear dipoles in the Apollo description.³⁰ Both simulations do show a preference for an Apollo-like structure in the $\theta = 0^{\circ}$ case, with chloroform's ordering being more diffuse. However, we note that the population of haloform pairs with the $\theta = 0^{\circ}$ configuration is very small compared other θ positions, as shown earlier in Figure 3b. These $\theta = 0^{\circ}$ contours lack evidence of head-to-head arrangement, shown as configuration (2) in Figure 5d. This is the largest deviation from recent ND-EPSR analyses, and we note that these recent interpretations have been inconsistent in regard to this aspect of

haloform ordering, with reports of nearest neighbor head-to-head orientation being more prevalent in chloroform but negligible in bromoform²⁹ and the reverse case, with more head-to-head orientation in bromoform.^{30,31}

Differences between chloroform and bromoform are apparent in the electrostatically-induced ordering at $\theta = 90^{\circ}$, $\alpha \approx 255^{\circ}$ where chloroform shows a noticeably stronger preference for this configuration due to Coulombic attraction between the neighboring H and reference Cl atoms. In contrast, the orientation of neighboring chloroform at $\theta = 0^{\circ}$ centered around $\alpha = 0^{\circ}$ is more diffuse in chloroform than in bromoform, suggesting that the ordering in this position, corresponding to configuration (1), is a stronger function of sterics than electrostatics, also supported by the q = 0 simulations shown in Figure S3.

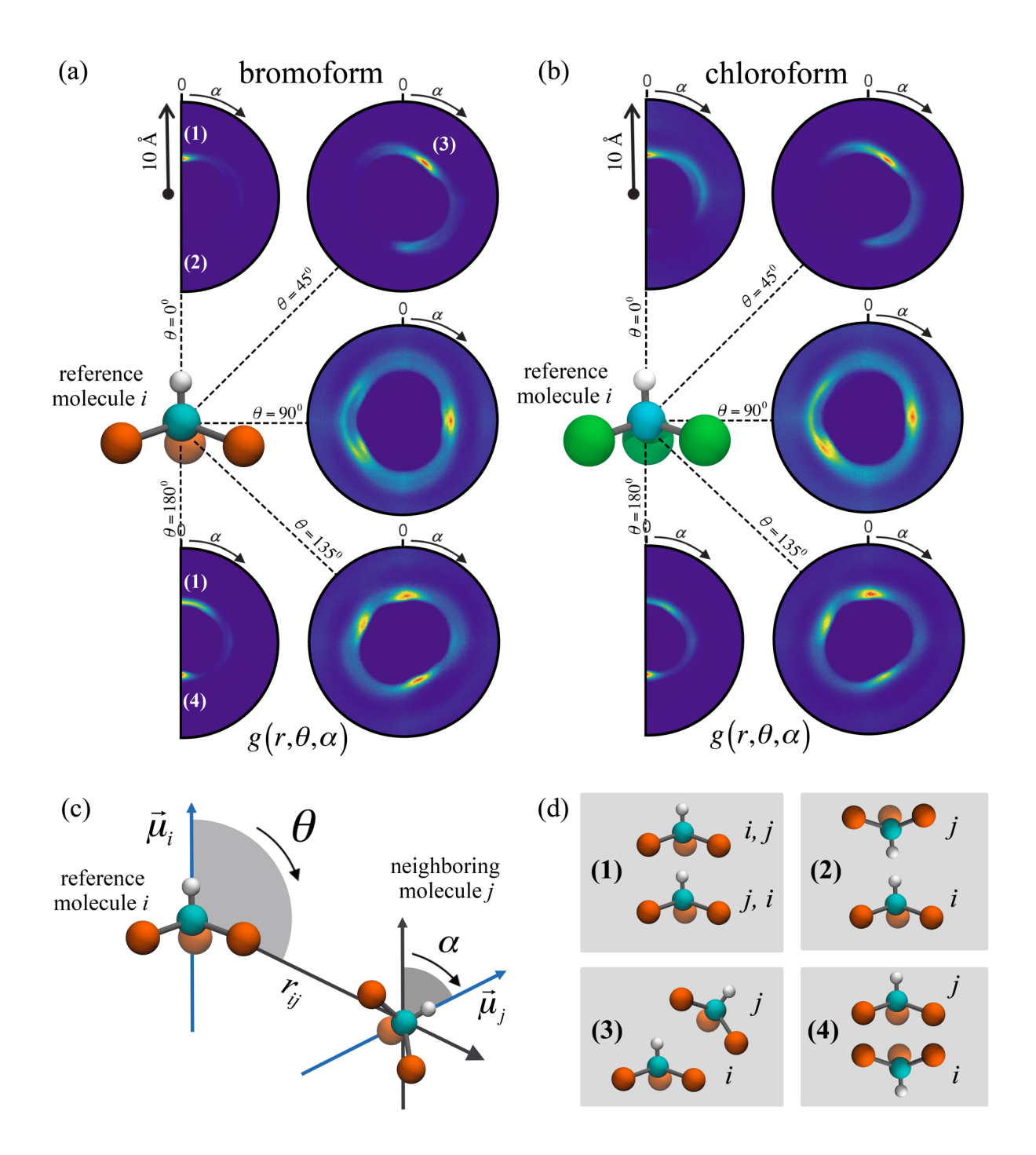


Figure 5. Dipole orientation contour plots for (a) bromoform and (b) chloroform show the orientation of neighboring dipoles (dipole-dipole angle α) as a function of center-of-mass separation and spatial position relative to the reference molecule's dipole vector (angle θ). Panel

(c) is a cartoon schematic that defines the variables r, θ , and α . Panel (d) shows the relative orientation of i-j pairs that correspond to the (1) – (4) labels in panel (a).

3.2 Orientational dynamics and structural lifetimes

We next consider the dynamics of the haloform liquids and define the dipole orientational correlation function, $C_o(t)$, as

$$C_o(t) = \frac{\langle \hat{\mu}(0) \cdot \hat{\mu}(t) \rangle}{\langle \hat{\mu}(0) \cdot \hat{\mu}(0) \rangle} \tag{4}$$

where $\hat{\mu}(\tau)$ is a unit vector parallel to haloform's dipole moment vector at time τ and the ensemble averages are collected for every haloform molecule and for all possible time origins. Figure 6a shows $C_o(t)$ decay curves, plotted for both neat liquids and for the corresponding q = 0simulations. The inset cartoon illustrates the dipole moment vectors $\vec{\mu}$ at times 0 and t. Bromoform reorientational dynamics are considerably slower than chloroform with single exponential decay constants of 10.33 and 5.46 ps respectively. Decay constants for all four $C_o(t)$ curves are collected in Table 3. Corresponding zero-charge simulations showed faster dynamics than their charged counterparts due to dielectric friction effects in the latter.⁴¹ One would expect slower dynamics in chloroform due to its bigger charges but bromoform and chloroform differ significantly in mass, which also influences the reorientational dynamics. In Figure 6b we remove mass effects by considering $I \ln(C_0(t))$, where I is the moment of inertia of the molecule. This modification deconvolutes charge separation and mass, revealing the expected trend with chloroform showing slower dynamics than bromoform. Additionally, as a self-consistency check, we note that the two zero-charge simulations have similar dynamics due to their similar geometries as expected. This multi-step deconstruction of haloform reorientational dynamics reveals an important and interesting feature of the molecular liquids. The haloform models'

partial charges differ by a significant amount. Despite these differences, the haloforms exhibit very similar intermolecular local ordering and structure but the greater charge separation in the chloroform model slows its orientational dynamics relative to bromoform.

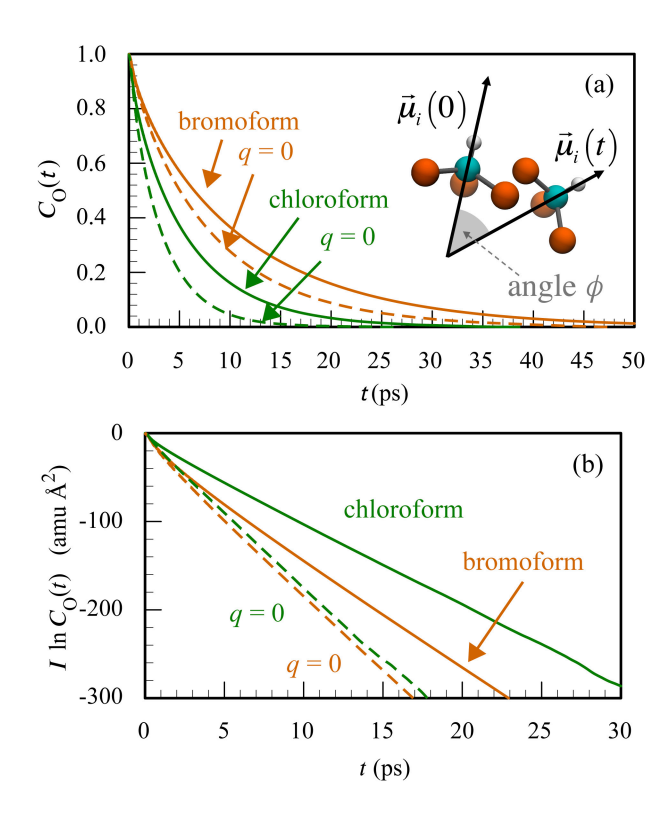


Figure 6. (a) Dipole orientational time correlation functions $C_o(t)$ for bromoform (orange) and chloroform (green). The inset cartoon defines the dipole angle ϕ . (b) $C_o(t)$ modified by the respective moment of inertia I to remove mass effects on molecular reorientation.

Table 3. Dipole orientational time constants τ for the haloforms and corresponding q=0 simulations.

system	τ (ps)
CFM	5.46
CFM, q = 0	3.16
BFM	10.33

BFM, $q = 0$	7.74

In Figure 7 we revisit the concept of the "polar stack" as defined by Salzmann and coworkers, 30 where neighboring haloform molecules are defined to participate in a polar stack structure if their C-H distance is between 2.0 and 4.2 Å and have an H-C···H angle between 150° and 210°. The population of molecules participating in these stacks is summarized in Figure 7a, where n = 2 indicates 2 molecules in a stack, n = 3 is a stack of 3, etc. and n = 1 represents molecules that do not participate in a stack. We emphasize that the polar stacks are not the major structural feature in haloform liquids (most molecules do not participate in a 'stack') and we do not suggest that these structures dictate any macroscopic properties or behavior. Quantification of this ordering is employed as a metric to directly compare our MD simulations with ND-EPSR results for liquid chloroform³⁰ and they agree well. The number of bromoform molecules participating in polar stacks may be overestimated by our simulations. Polar stacking was not quantified in the more recent ND-EPSR studies of bromoform, but Salzmann and co-workers state that bromoform shows evidence of polar stacking and the structures may be present in lower populations than chloroform due to more antiparallel dipole alignment detected in bromoform.³¹ Our simulations suggest that the ordering which results in these polar stacks is driven by steric packing since the zero charge simulations show only slightly smaller stack populations (i.e. $n \ge 2$) and the two haloforms, with different charge separations but similar geometries, report nearly identical polar stacking population distributions. These results refute the earlier, intuitive suggestion that this ordering be driven by electrostatics.²⁷

We also consider the lifetime of the polar stacks, a convenient metric to further investigate the local dynamics of the haloform liquids. To quantify these lifetimes, we scan the MD trajectory

on-the-fly for haloform molecules that fit the geometrical definition of polar stacking and track these polar stacks as the simulations progress. For each stack, we define the variable $h(\tau)$ to be 1 if the stack is present at a given timestep τ and 0 if it does not fit the geometrical criteria. With this dynamic population information we calculate lifetime correlation functions for the polar stacks as

$$C_{\lambda}(t) = \frac{\langle h(0) \cdot h(t) \rangle}{\langle h(0) \cdot h(0) \rangle} \tag{5}$$

where the ensemble average is collected for all detected polar stacks and all possible time origins. Figure 7b shows these correlation functions, $C_A(t)$, for the two haloform systems and their zero charge analogs. Two $C_A(t)$ curves are shown for each system, separated into two categories that represent all stacks $n \ge 2$ and larger stacks $n \ge 3$, indicated by the arrows in Figure 7b. The stack lifetimes agree with the reorientational dynamics in Figure 6a, with bromoform stacks being longer lived than chloroform for both the large and small population samples. This result is expected when considering the reorientational dynamics but the $C_A(t)$ of the zero charge systems is less intuitive and suggests that the breakup of the polar stacks is a dynamic event not related to electrostatics.

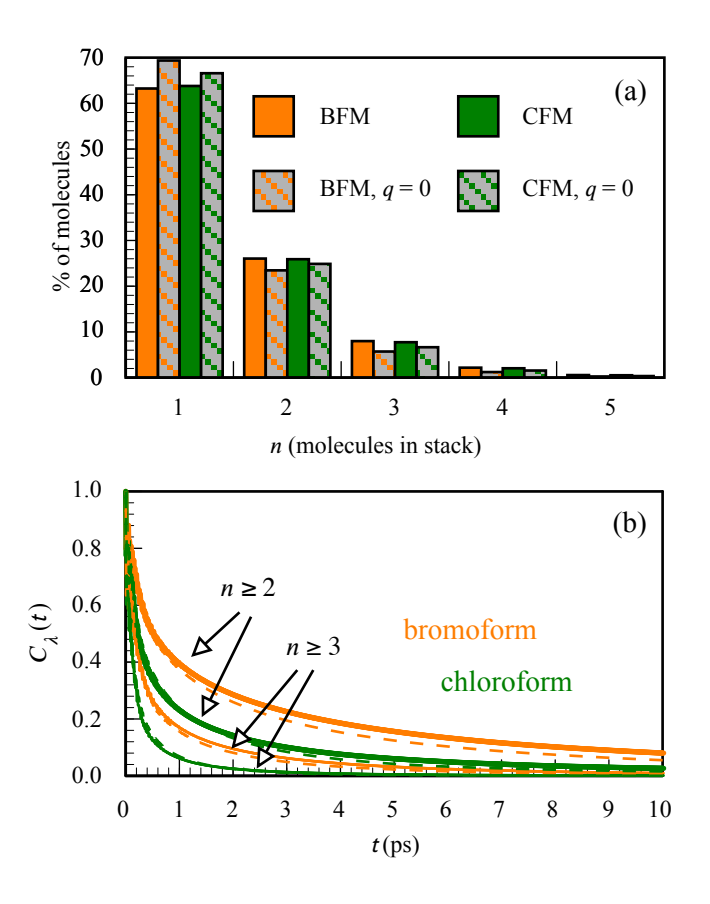


Figure 7. (a) 'Polar stacking' populations and (b) stack lifetime correlation functions, $C_{\lambda}(t)$, for chloroform (green) and bromoform (orange). Lifetime correlations are separated to describe short $(n \ge 2)$ and long $(n \ge 3)$ polar stacks. Dashed curves represent the corresponding $C_{\lambda}(t)$ for q = 0 simulations.

4. Conclusions

Using structural and dynamical analysis on two structurally similar liquids we are able to gain important insight into the factors that produce observed ordering in the two polar liquids, in good agreement with recent ND-EPSR results. Spatial distribution functions reveal that the first peaks in the radial distribution functions are composed of several localized high-density regions that correspond to steric packing of the nearly-tetrahedral molecular liquids, electrostatics having a

significantly smaller effect on the local structure. Dipole orientational contour plots show a strong preference for neighboring molecules' dipoles to be parallel to the vector connecting the centers of mass and pointing away from the reference molecule. Electrostatic interactions, stronger in chloroform than bromoform, result in other preferred dipole-dipole orientations. These contour plots also reveal the presence of tail-tail ordering, with colinear and antiparallel dipoles, in agreement with earlier diffraction experiments. The populations of 'polar stacks,' chains of haloforms arranged head-to-tail, are remarkably similar, suggesting that these structures result from steric packing effects and that bromoform 'polar stacks' are longer lived. Reorientational dynamics of liquid bromoform are slower than chloroform, despite chloroform's larger charge separation. The larger mass of bromoform has a greater effect on reorientational dynamics than corresponding dielectric friction effects.

ASSOCIATED CONTENT

Supporting Information. Comparison of normal and q = 0 simulations, dipole orientation contour plots for the q = 0 and standard simulations, and additional discussion regarding force field selection. (PDF)

AUTHOR INFORMATION

Corresponding Authors

*karnes@llnl.gov, ilan@ucsc.edu

Author Contributions

The manuscript was written through contributions of all authors. All authors have given approval to the final version of the manuscript.

ACKNOWLEDGMENTS

This work was supported by Lawrence Livermore National Laboratory's Laboratory-Directed Research and Development (LDRD) funding, Project No. 21-ERD-013, and performed under the auspices of the U.S. Department of Energy by Lawrence Livermore National Laboratory under Contract DE-AC52-07NA27344, release number LLNL-JRNL-816716-DRAFT. (J.J.K.) This work was supported by the National Science Foundation through grants CHE-1363076 and CHE-1800158. (I.B.) J.J.K. thanks J. S. Oakdale and J. D. Kemper for insightful comments and conversations during the preparation of this manuscript.

REFERENCES

- (1) Lark-Horovitz, K.; Miller, E. P. Structure of Liquid Argon. *Nature* **1940**, *146* (3701), 459–460. https://doi.org/10.1038/146459b0.
- (2) Reekie, J.; Hutchison, T. S. The Structure of Liquid Helium. *Phys. Rev.* **1953**, 92 (3), 827–828. https://doi.org/10.1103/PhysRev.92.827.2.
- (3) Achter, E. K.; Meyer, L. X-Ray Scattering from Liquid Helium. *Phys. Rev.* **1969**, *188* (1), 291–300. https://doi.org/10.1103/PhysRev.188.291.
- (4) Powles, J. G. The Structure of Molecular Liquids by Neutron Scattering. *Adv. Phys.* 1973,
 22 (1), 1–56. https://doi.org/10.1080/00018737300101259.
- (5) Hansen, J.-P.; McDonald, I. R. Theory of Simple Liquids; Academic Press: San Diego, 1990.

- (6) Soper, A. K. Orientational Correlation Function for Molecular Liquids: The Case of Liquid Water. *J. Chem. Phys.* **1994**, *101* (8), 6888–6901. https://doi.org/10.1063/1.468318.
- (7) Fuchizaki, K.; Sakagami, T.; Kohara, S.; Mizuno, A.; Asano, Y.; Hamaya, N. Structure of a Molecular Liquid GeI ₄. *J. Phys. Condens. Matter* **2016**, 28 (44), 445101. https://doi.org/10.1088/0953-8984/28/44/445101.
- (8) Sakagami, T.; Fuchizaki, K. Does a Network Structure Exist in Molecular Liquid SnI4 and GeI4? *J. Phys. Condens. Matter* **2017**, 29 (14), 145102. https://doi.org/10.1088/1361-648X/aa5f09.
- (9) Skinner, L. B.; Galib, M.; Fulton, J. L.; Mundy, C. J.; Parise, J. B.; Pham, V.-T.; Schenter, G. K.; Benmore, C. J. The Structure of Liquid Water up to 360 MPa from X-Ray Diffraction Measurements Using a High Q-Range and from Molecular Simulation. J. Chem. Phys. 2016, 144 (13), 134504. https://doi.org/10.1063/1.4944935.
- (10) Leonhardi, T. C.; Militzer, B. Ab Initio Simulations of Liquid Carbon Monoxide at High Pressure. *High Energy Density Phys.* **2017**, 22, 41–45. https://doi.org/10.1016/j.hedp.2017.02.005.
- (11) Naserifar, S.; Goddard, W. A. The Quantum Mechanics-Based Polarizable Force Field for Water Simulations. *J. Chem. Phys.* **2018**, *149* (17), 174502. https://doi.org/10.1063/1.5042658.
- (12) Wang, H.; Yang, W. Force Field for Water Based on Neural Network. *J. Phys. Chem. Lett.* 2018, 9 (12), 3232–3240. https://doi.org/10.1021/acs.jpclett.8b01131.

- (13) Magdău, I. B.; Mead, G. J.; Blake, G. A.; Miller, T. F. Interpretation of the THz-THz-Raman Spectrum of Bromoform. *J. Phys. Chem. A* **2019**, *123* (33), 7278–7287. https://doi.org/10.1021/acs.jpca.9b05165.
- (14) Basma, N. S.; Headen, T. F.; Shaffer, M. S. P.; Skipper, N. T.; Howard, C. A. Local Structure and Polar Order in Liquid *N* -Methyl-2-Pyrrolidone (NMP). *J. Phys. Chem. B* **2018**, *122* (38), 8963–8971. https://doi.org/10.1021/acs.jpcb.8b08020.
- (15) Besford, Q. A.; Christofferson, A. J.; Liu, M.; Yarovsky, I. Long-Range Dipolar Order and Dispersion Forces in Polar Liquids. *J. Chem. Phys.* **2017**, *147* (19), 194503. https://doi.org/10.1063/1.5005581.
- (16) Chandler, D. Equilibrium Structure and Molecular Motion in Liquids. *Acc. Chem. Res.* **1974**, 7 (8), 246–251. https://doi.org/10.1021/ar50080a002.
- (17) Chandler, D. Structures of Molecular Liquids. *Annu. Rev. Phys. Chem.* 1978, 29, 441–471.https://doi.org/10.1146/annurev.pc.29.100178.002301.
- (18) Chandler, D.; Weeks, J. D. Equilibrium Structure of Simple Liquids. *Phys. Rev. Lett.* 1970, 25 (3), 149–152. https://doi.org/10.1103/PhysRevLett.25.149.
- (19) Weeks, J. D.; Chandler, D.; Andersen, H. C. Role of Repulsive Forces in Determining the Equilibrium Structure of Simple Liquids. *J. Chem. Phys.* **1971**, *54* (12), 5237–5247. https://doi.org/10.1063/1.1674820.
- (20) Andersen, H. C.; Chandler, D.; Weeks, J. D. Roles of Repulsive and Attractive Forces in Liquids: The Equilibrium Theory of Classical Fluids. In *Advances in Chemical Physics*; John Wiley & Sons, Ltd, 1976; pp 105–156. https://doi.org/10.1002/9780470142530.ch2.

- (21) Hoheisel, C.; Zeidler, M. D. The Radial Pair-Distribution Function of Liquid CHCl3.

 *Berichte Bunsenges. Für Phys. Chem. 1979, 83 (1), 28–29.

 https://doi.org/10.1002/bbpc.19790830106.
- (22) Chang, T.-M.; Dang, L. X.; Peterson, K. A. Computer Simulation of Chloroform with a Polarizable Potential Model. *J. Phys. Chem. B* **1997**, *101* (17), 3413–3419. https://doi.org/10.1021/jp9638550.
- (23) Chang, T.-M.; Dang, L. X. Ion Solvation in Polarizable Chloroform: A Molecular Dynamics Study. *J. Phys. Chem. B* **1997**, *101* (49), 10518–10526. https://doi.org/10.1021/jp972101y.
- (24) Lamoureux, G.; Faraldo-Gómez, J. D.; Krupin, S.; Noskov, S. Y. Polarizable Model of Chloroform Based on Classical Drude Oscillators. *Chem. Phys. Lett.* **2009**, *468* (4–6), 270–274. https://doi.org/10.1016/j.cplett.2008.12.002.
- (25) Pothoczki, S.; Temleitner, L.; Pusztai, L. Structure of Neat Liquids Consisting of (Perfect and Nearly) Tetrahedral Molecules. *Chem. Rev.* **2015**, *115* (24), 13308–13361. https://doi.org/10.1021/acs.chemrev.5b00308.
- (26) Bertagnolli, H.; Leicht, D. O.; Zeidler, M. D.; Chieux, P. A Neutron Diffraction Study of Liquid Chloroform. *Mol. Phys.* 1978, 36 (6), 1769–1777. https://doi.org/10.1080/00268977800102751.
- (27) Bertagnolli, H.; Chieux, P. The Complete Set of Atom Pair Correlation Functions of Liquid Chloroform as Obtained from a Final Neutron Scattering Experiment with H/D Isotopic Substitution. *Mol. Phys.* **1984**, *51* (3), 617–631. https://doi.org/10.1080/00268978400100431.

- (28) Pothoczki, S.; Temleitner, L.; Kohara, S.; Jóvári, P.; Pusztai, L. The Liquid Structure of Haloforms CHCl₃ and CHBr₃. *J. Phys. Condens. Matter* **2010**, 22 (40), 404211. https://doi.org/10.1088/0953-8984/22/40/404211.
- (29) Pothoczki, S.; Temleitner, L.; Pusztai, L. Detailed Intermolecular Structure of Molecular Liquids Containing Slightly Distorted Tetrahedral Molecules with C_{3v} Symmetry: Chloroform, Bromoform, and Methyl-Iodide. *J. Chem. Phys.* **2011**, *134* (4), 044521. https://doi.org/10.1063/1.3517087.
- (30) Shephard, J. J.; Soper, A. K.; Callear, S. K.; Imberti, S.; Evans, J. S. O.; Salzmann, C. G. Polar Stacking of Molecules in Liquid Chloroform. *Chem. Commun.* **2015**, *51*, 4770–4773. https://doi.org/10.1039/C4CC09235J.
- (31) Shephard, J. J.; Evans, J. S. O.; Salzmann, C. G. Local Structure and Orientational Ordering in Liquid Bromoform. *Mol. Phys.* **2019**, *117* (22), 3337–3344. https://doi.org/10.1080/00268976.2019.1648897.
- (32) Bertagnolli, H.; Goller, K.; Zweier, H. Structure Investigations of Liquid Chloroform by Statistical-Mechanical Calculations and Reverse Monte Carlo Simulation. *Berichte Bunsenges*. *Für Phys. Chem.* **1995**, 99 (10), 1168–1178. https://doi.org/10.1002/bbpc.199500056.
- (33) Karnes, J. J.; Benjamin, I. On the Local Intermolecular Ordering and Dynamics of Liquid Chloroform. *J. Mol. Liq.* **2017**, 248 (Supplement C), 121–126. https://doi.org/10.1016/j.molliq.2017.10.023.
- (34) Jorgensen, W. L.; Tirado-Rives, J. Potential Energy Functions for Atomic-Level Simulations of Water and Organic and Biomolecular Systems. *Proc. Natl. Acad. Sci. U. S. A.* **2005**, *102* (19), 6665–6670. https://doi.org/10.1073/pnas.0408037102.

- (35) Storer, J. W.; Giesen, D. J.; Cramer, C. J.; Truhlar, D. G. Class IV Charge Models: A New Semiempirical Approach in Quantum Chemistry. *J. Comput. Aided Mol. Des.* **1995**, *9* (1), 87–110. https://doi.org/10.1007/BF00117280.
- (36) Dodda, L. S.; Cabeza de Vaca, I.; Tirado-Rives, J.; Jorgensen, W. L. LigParGen Web Server: An Automatic OPLS-AA Parameter Generator for Organic Ligands. *Nucleic Acids Res.* **2017**, *45* (W1), W331–W336. https://doi.org/10.1093/nar/gkx312.
- (37) Dodda, L. S.; Vilseck, J. Z.; Tirado-Rives, J.; Jorgensen, W. L. 1.14*CM1A-LBCC: Localized Bond-Charge Corrected CM1A Charges for Condensed-Phase Simulations. *J. Phys. Chem. B* **2017**, *121* (15), 3864–3870. https://doi.org/10.1021/acs.jpcb.7b00272.
- (38) Ding, F.; Hu, Z. H.; Zhong, Q.; Manfred, K.; Gattass, R. R.; Brindza, M. R.; Fourkas, J. T.; Walker, R. A.; Weeks, J. D. Interfacial Organization of Acetonitrile: Simulation and Experiment. J. Phys. Chem. C 2010, 114 (41), 17651–17659. https://doi.org/10.1021/Jp104597z.
- (39) Pothoczki, S.; Ottochian, A.; Rovira-Esteva, M.; Pardo, L. C.; Tamarit, J. L.; Cuello, G. J. Role of Steric and Electrostatic Effects in the Short-Range Order of Quasitetrahedral Molecular Liquids. *Phys. Rev. B* 2012, 85 (1), 014202. https://doi.org/10.1103/PhysRevB.85.014202.
- (40) Lowden, L. J.; Chandler, D. Theory of Intermolecular Pair Correlations for Molecular Liquids. Applications to the Liquids Carbon Tetrachloride, Carbon Disulfide, Carbon Diselenide, and Benzene. J. Chem. Phys. 1974, 61 (12), 5228–5241. https://doi.org/10.1063/1.1681868.
- (41) Fleming, G. R. *Chemical Applications of Ultrafast Spectroscopy*; International Series of Monographs on Chemistry; Oxford University Press: New York, 1986.

For Table of Contents Only

